nature catalysis

Article

https://doi.org/10.1038/s41929-024-01229-x

Ammonia synthesis via an engineered nitrogenase assembly pathway in *Escherichia coli*

Received: 31 January 2024

Accepted: 19 August 2024

Published online: 19 September 2024

Check for updates

Joseph B. Solomon[1,2,3], Chi Chung Lee[1,3], Yiling A. Liu[1], Calder Duffin[1,2], Markus W. Ribbe[1,2] ✉ & Yilin Hu[1] ✉

Heterologous expression of nitrogenase has been actively pursued because of the far-reaching impact of this enzyme on agriculture, energy and the environment. However, isolation of an active two-component, metallocentre-containing nitrogenase from a non-diazotrophic host has yet to be accomplished. Here we report the heterologous synthesis of an active molybdenum-nitrogenase by combining genes from *Azotobacter vinelandii* and *Methanosarcina acetivorans* in *Escherichia coli*. Metal, activity and electron paramagnetic resonance analyses demonstrate the integrity of the metallocentres in the purified nitrogenase enzyme; whereas growth, nanoscale secondary ion mass spectrometry and nuclear magnetic resonance experiments illustrate diazotrophic growth and ^{15}N enrichment by the *E. coli* expression strain, and accumulation of extracellular ammonia upon deletion of the ammonia transporter that permits incorporation of thus-generated nitrogen into the cellular mass of a non-diazotrophic *E. coli* strain. As such, this study provides a crucial prototype system that could be optimized/modified to enable future transgenic expression and biotechnological adaptations of nitrogenase.

Nitrogenase plays a key role in the nitrogen cycle on Earth, catalysing the remarkable conversion of N_2 to NH_3 in an ambient process called biological nitrogen fixation[1]. Additionally, nitrogenase can reduce a variety of small molecules, including CO, C_2H_2, CN^- and N_3^-, under ambient conditions[2–4]. Notably, the reduction of CO to hydrocarbons (for example, C_2H_4, C_2H_6, C_3H_6, C_3H_8) by nitrogenase[5,6] is analogous to the reduction of N_2 to NH_3 by the same enzyme[1]; both of these processes utilize ATP as the energy source and H^+/e^- as the reducing equivalent to drive the reaction. Moreover, the enzymatic CO and N_2 reduction by nitrogenase mirror the industrial Fischer–Tropsch[7,8] and Haber–Bosch[9,10] processes for the large-scale production of liquid carbon fuels and ammonia, respectively; yet, unlike their industrial counterparts, the nitrogenase-catalysed reactions occur under ambient conditions and do not consume the expensive H_2 gas[1,6]. The distinct features of the nitrogenase-based reactions make this enzyme a logical candidate for heterologous expression in genetically amenable hosts, such as *Escherichia coli*, for the future development of bioreactors to harness the reducing prowess of nitrogenase. Coupled with efforts to seek cheaper, renewable feedstocks to supply energy for the nitrogenase reactions, and taking advantage of H_2 being generated as an abundant by-product instead of being consumed as a substrate, the successful development of such nitrogenase-based bioreactors could potentially offer energy- and cost-efficient alternatives that complement traditional approaches for the production of high-value chemical commodities.

Encoded by *nif* genes, the conventional molybdenum (Mo)-nitrogenase has remained a focal point of efforts to heterologously synthesize nitrogenase in non-diazotrophic organisms. The best-characterized Mo-nitrogenase from *Azotobacter vinelandii* (Supplementary Fig. 1) consists of a reductase component and a catalytic component[11,12]. The reductase component, termed the Fe protein

[1]Department of Molecular Biology and Biochemistry, University of California, Irvine, Irvine, CA, USA. [2]Department of Chemistry, University of California, Irvine, Irvine, CA, USA. [3]These authors contributed equally: Joseph B. Solomon, Chi Chung Lee. ✉e-mail: mribbe@uci.edu; yilinh@uci.edu

(or NifH), is a γ_2-homodimer that has a [Fe_4S_4] cluster bridged at the subunit interface and a MgATP-binding site located within each subunit; the catalytic component, termed the MoFe protein (or NifDK), is an $\alpha_2\beta_2$-tetramer that has a P-cluster ([Fe_8S_7]) bridged at each α/β-subunit interface and an M-cluster (also known as FeMoco or cofactor; [(*R*-homocitrate)$MoFe_7S_9C$]) located within each α-subunit[13–17]. Catalysis by Mo-nitrogenase involves repeated association and dissociation of its two components, which facilitates the formation of an electron transport chain within the NifH/NifDK complex that extends from the [Fe_4S_4] cluster of NifH, through the P-cluster, to the M-cluster of NifDK, where substrate reduction takes place (Supplementary Fig. 1)[11,13,14].

Biosynthesis of Mo-nitrogenase (Supplementary Fig. 2)[3,18–20] is a highly involved process that centres on the formation of its P- and M-clusters, arguably two of the most complex, high-nuclearity metalloclusters found in biological systems. The assembly processes of both the P- and M-clusters begin with the synthesis of small [Fe_4S_4] building blocks by NifS (a cysteine desulfurase) and NifU (an FeS assembly scaffold); however, the two pathways branch at this point, with a pair of [Fe_4S_4] clusters delivered to NifDK (the catalytic component) and NifB (a cofactor assembly protein), respectively, for the assembly of P- and M-clusters (Supplementary Fig. 2a,b). The assembly of the P-cluster (Supplementary Fig. 2a) continues in situ (on-site) at its target location, where the [Fe_4S_4] cluster pair (designated the P*-cluster) are coupled into a [Fe_8S_7] cluster (that is, the P-cluster) at the α/β-subunit interface of NifDK[21–26]. Such a process results in a P-cluster-replete, yet M-cluster depleted apo NifDK, ready to receive the externally synthesized M-cluster. The assembly of the M-cluster (Supplementary Fig. 2b), on the other hand, occurs ex situ (off-site) outside its target location, where the [Fe_4S_4] cluster pair (designated the K-cluster) are coupled/rearranged into a [Fe_8S_9C] cluster (designated the L-cluster) via radical chemistry on NifB (a radical SAM enzyme) concomitant with the incorporation of a sulfite-derived ninth belt-sulfur[27–33]. The L-cluster is then transferred to NifEN (a cofactor assembly protein), where it undergoes transformation into a mature M-cluster upon NifH-mediated substitution of one terminal Fe of the L-cluster with Mo/homocitrate[34–39]. This event is followed by transfer of the M-cluster to its target binding site within the α-subunit of apo NifDK[23,36], resulting in a P- and M-cluster-replete, holo NifDK (Supplementary Fig. 2c).

The intricacy of the biosynthetic processes of both P- and M-clusters poses a serious challenge for the successful heterologous expression of Mo-nitrogenase in a non-diazotrophic host, such as *E. coli*. To circumvent this problem, we dedicated our efforts towards narrowing down the essential *nif* gene products through studies of purified assembly components from *A. vinelandii*, which led to the unambiguous identification of *nifS,U,H,M,Z,D,K,E,N,B,V* as the minimum set of essential genes that are required alongside the gene encoding an appropriate electron donor (for example, *fdxN*) for the expression of an active Mo-nitrogenase in this native diazotrophic host. Building on this knowledge, we then mixed and matched *nif* and related genes from *A. vinelandii* and those from a methanogenic organism, *Methanosarcina acetivorans*, for the heterologous expression and functional studies of key components of nitrogenase in *E. coli*[28–33,40,41]. Most importantly, our recent efforts led to the successful heterologous synthesis of three proteins: (1) a [Fe_4S_4] cluster-replete NifH (Fig. 1, coloured dark blue) derived from coexpression of *nifH,M* with *iscS,U* of *A. vinelandii* in *E. coli*, which is fully active in catalysis and assembly[42]; (2) a P-cluster-replete, but M-cluster-depleted apo NifDK (designated $NifDK^{apo}$; Fig. 1, coloured green)[43] derived from coexpression of *nifH,M,Z,D,K* with *iscS,U* of *A. vinelandii* in *E. coli*, which can be activated upon cofactor incorporation; (3) an L-cluster-containing NifB protein (Fig. 1, coloured yellow)[43] derived from coexpression of *nifS3,U3,B* of *M. acetivorans* with *fdxN* of *A. vinelandii* in *E. coli*, which can serve as a cofactor source upon the L- to M-cluster conversion on NifEN. More importantly, we purified these heterologously expressed nitrogenase proteins and verified the formation of the metallocentres and, in particular, the P- and L-clusters, on these proteins through metalloprotein-specific biochemical (metal, activity) and spectroscopic (electron paramagnetic resonance (EPR), X-ray absorption spectroscopy/extended X-ray absorption fine structure) analyses, thereby validating our model of nitrogenase assembly while providing conclusive evidence for the feasibility of synthesizing the complex metallocentres of nitrogenase in a non-diazotrophic host, such as *E. coli*[42,43].

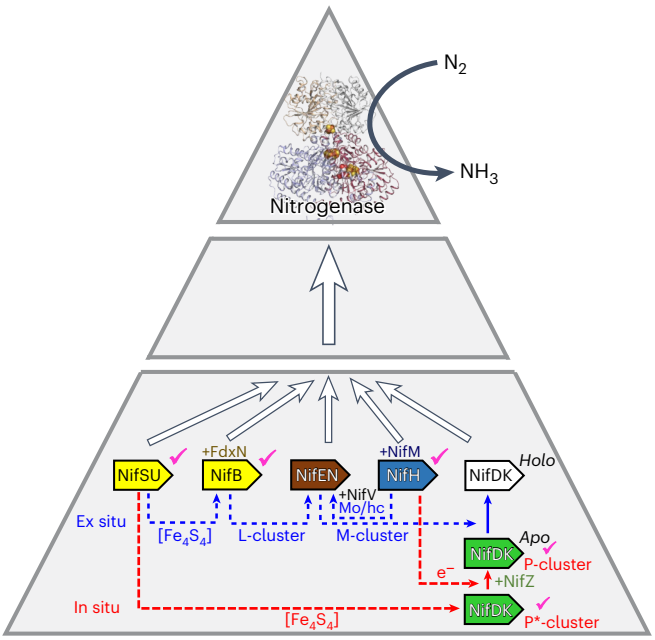

Fig. 1 | A bottom-up metallocentric approach to heterologously express nitrogenase. Biosynthesis of Mo-nitrogenase consists of two components: (1) the in situ assembly of the P-cluster, which involves fusion of a [Fe_4S_4] cluster pair into a P-cluster ([Fe_8S_7]) on NifDK that results in a P-cluster-containing, yet M-cluster-deficient $NifDK^{apo}$ (red arrows); and (2) the ex situ assembly of the M-cluster, which involves coupling/rearrangement of a [Fe_4S_4] cluster pair into an L-cluster ([Fe_8S_9C]) on NifB concomitant with insertion of an interstitial carbon and a ninth sulfur, maturation of the L-cluster into an M-cluster ([(*R*-homocitrate)$MoFe_7S_9C$]) on NifEN via NifH-mediated Mo/homocitrate (hc) insertion, and delivery of the M-cluster to $NifDK^{apo}$ that results in a P- and M-cluster containing $NifDK^{holo}$ (blue arrows). Our recent success with the heterologous expression and biochemical/spectroscopic characterization of a P-cluster containing $NifDK^{apo}$ (green), an L-cluster containing NifB (yellow) and an [Fe_4S_4] cluster containing NifH (dark blue) in *E. coli* have implemented critical checkpoints along the biosynthetic pathway (indicated by √) to verify the heterologous synthesis of the complex metallocentres of nitrogenase. Building on these results, an M-cluster containing NifEN (dark brown) can be implemented as the final checkpoint prior to combining all essential biosynthetic components for the heterologous expression of a complete Mo-nitrogenase. Such a metallocentric, divide-and-conquer approach allows for a bottom-up construction of a biosynthetic pathway of nitrogenase in any foreign host and highlights the necessity to demonstrate the heterologous expression of nitrogenase via analysis of the metallocluster content and functional competence of the purifiable nitrogenase components.

The successful expression of the P-cluster-containing apo NifDK and the L-cluster-containing NifB in *E. coli* illustrates the effectiveness of individually addressing the biosynthetic competence of the key intermediates of nitrogenase assembly before combining these events for the heterologous expression of a complete nitrogenase. Such a metallocentric, divide-and-conquer approach allows for a strategic implementation of two crucial checkpoints along the biosynthetic pathway of nitrogenase and a conclusive demonstration of cluster formation via analyses of purified proteins, a concept that has not been considered in previous efforts[44–46] that centred on a one-shot,

https://doi.org/10.1038/s41929-024-01229-x

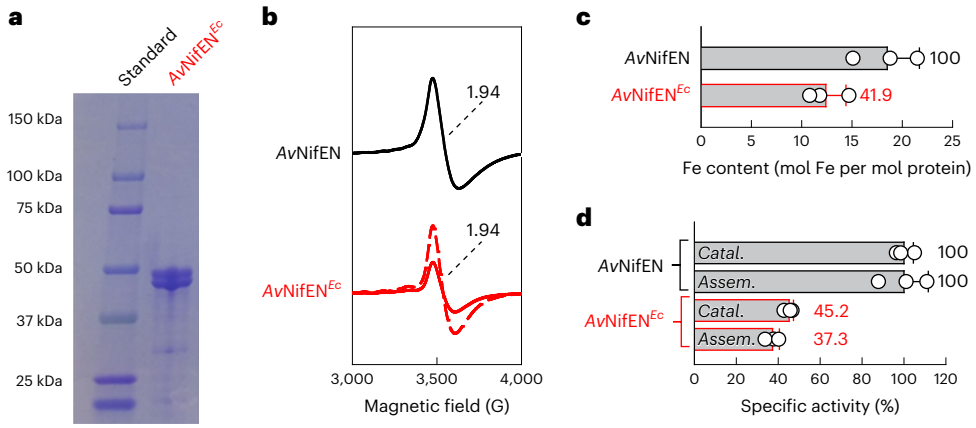

Fig. 2 | Biochemical and spectroscopic analyses of *Av*NifEN^{Ec}. **a**, SDS-PAGE of the as-isolated *Av*NifEN^{Ec}. Shown is a representative image of three independent experiments with reproducible results. Heterologously expressed in *E. coli* strain YM577EE (Supplementary Table 2), *Av*NifEN^{Ec} is a heterotetramer composed of α- and β-subunits of ~50 kDa and ~49 kDa, respectively. Standard, Precision Plus Protein Kaleidoscope prestained protein standards (Bio-Rad). **b**, Perpendicular mode EPR spectra of the IDS-oxidized *Av*NifEN and *Av*NifEN^{Ec}. Also shown is the L-cluster specific EPR signal of *Av*NifEN^{Ec} at $g = 1.94$, with its signal intensity normalized based on the L-cluster content (red dashed line). **c**, Fe analyses of *Av*NifEN and *Av*NifEN^{Ec}. The L-cluster content of *Av*NifEN or *Av*NifEN^{Ec} was calculated by subtracting eight Fe atoms in the two permanent [Fe_4S_4] clusters from the total amount of Fe atoms per NifEN tetramer. The relative L-cluster content of *Av*NifEN^{Ec} (expressed as a percentage) as compared to that of *Av*NifEN (set as 100%) is indicated in red font. **d**, Activity analyses of *Av*NifEN and *Av*NifEN^{Ec} in catalysis (Catal.) and M-cluster assembly (Assem.). The relative activities of *Av*NifEN^{Ec} (expressed as percentages) compared with those of *Av*NifEN (set as 100%) are indicated in red font. See Supplementary Table 3 for details on Fe contents and specific activities. The error bars represent the standard deviation from the mean, originating from three independent Fe analyses (**c**) and three independent activity analyses (**d**) of each of *Av*NifEN^{Ec} and *Av*NifEN.

whole-gene-set transfer for the heterologous expression of nitrogenase, followed by whole-cell analysis of the functionality of this enzyme. With the heterologous synthesis of the high-nuclearity, homometallic cores of P- and L-clusters accomplished in the heterologously expressed NifDK and NifB proteins[43], respectively, we have overcome two major hurdles for the heterologous expression of nitrogenase and are poised to extend the cofactor assembly pathway for the heterologous expression of a holo NifDK species in *E. coli*. Specifically, by adding the biosynthetic components required for cofactor maturation (that is, *nifE,N,V*) to those for the expression of NifB and apo NifDK (that is, *nifS,U,B,fdxN* and *nifH,M,Z,D,K*), we should be able to generate a system wherein the L-cluster is transferred from NifB to NifEN and matured into an M-cluster prior to the delivery of the M-cluster to apo NifDK.

Here we report the heterologous formation of an active Mo-nitrogenase of *A. vinelandii* in *E. coli* upon coexpression of *A. vinelandii nifH,M,Z,D,K,E,N,V* and *fdxN* genes along with *M. acetivorans nifS3,U3,B* genes (see Supplementary Table 1 for alternative designations of *Ma nifS3* (gene symbol/ID: MA0808/638175558) and *Ma nifU3* (gene symbol/ID: MA0807/638175557))[47]. Combined metal, activity and EPR analyses of the two purified components of the heterologously expressed Mo-nitrogenase reveal the presence of 90% and 34%, respectively, of the as-isolated NifH and NifDK in a cluster-replete, holo conformation. Moreover, cell growth and nanoscale secondary ion mass spectrometry (nanoSIMS) experiments demonstrate the ability of the nitrogenase-expressing *E. coli* strain to sustain diazotrophic growth and incorporate $^{15}N_2$-derived, fixed nitrogen into the cell mass upon exhaustion of a limited amount of ammonia in the growth medium. Finally, frequency-selective nuclear magnetic resonance (NMR) analysis shows accumulation of extracellular ammonia upon deletion of *amtB*, the gene encoding the ammonia transporter protein AmtB, in the genome of the nitrogenase-expressing *E. coli* strain; and nanoSIMS analysis illustrates a 4.3-fold ^{15}N enrichment in a nitrogenase-free *E. coli* strain upon incubation with the supernatant of the Δ*amtB* nitrogenase-expressing *E. coli* strain prepared with $^{15}N_2$. Together, these observations not only establish our diazotrophic *E. coli* strain as a prototype for further optimization of nitrogenase expression, but also point to the utility of this heterologous expression system as a potential template for future biotechnological adaptations of nitrogenase-based applications.

Results

Heterologous expression of an L-cluster-bound NifEN

We began our effort towards the heterologous expression of a complete Mo-nitrogenase in *E. coli* by expressing an L-cluster-containing NifEN as the last checkpoint along the biosynthetic pathway of NifDK (see Fig. 1, dark brown). This objective was necessary because the feasibility of an in vivo transfer of L-clusters from NifB to NifEN had not been established in this foreign host. As shown in Fig. 2, coexpression of the *nifE*(*his*-tagged),*N* and *fdxN* genes from *A. vinelandii* (*Av*) and the *nifS3,U3,B* genes from *M. acetivorans* (*Ma*) in *E. coli* strain MY21, a BL21(DE3)-derived Δ*iscR* strain, resulted in the heterologous synthesis of a soluble, brown His-tagged NifEN species (designated *Av*NifEN^{Ec}). Isolated at a yield of 600 mg per 100 g wet cells, *Av*NifEN^{Ec} is an $\alpha_2\beta_2$-tetramer comprising α- and β-subunits of ~50 kDa and ~49 kDa, respectively (Fig. 2a). Moreover, like the native *Av*NifEN, *Av*NifEN^{Ec} displays a $g = 1.94$ EPR signal that is characteristic of the L-cluster in the oxidized state[34], although the signal intensity of *Av*NifEN^{Ec} is ~38% of that of its native counterpart (Fig. 2b). Consistent with this observation, *Av*NifEN^{Ec} shows an L-cluster-specific Fe content of 41.9% (Fig. 2c), a C_2H_2-reducing activity of 45.2% (Fig. 2d, Catal.) and an L- to M-cluster maturation activity of 37.3% (Fig. 2d, Assem.), relative to those of the native *Av*NifEN, all of which point to an L-cluster content of *Av*NifEN^{Ec} that is ~40% of that of its native counterpart. Such an L-cluster occupancy of *Av*NifEN^{Ec} indicates a good efficiency of in vivo L-cluster transfer between *Ma*NifB and *Av*NifEN, which is particularly encouraging given the cross-species interaction between the two proteins and the necessity to express *Ma*NifB instead of its homologous *Av*NifB counterpart due to the challenge of expressing the latter in *E. coli*.

Heterologous synthesis of a complete Mo-nitrogenase

Having established the feasibility of cluster transfer between NifB and NifEN, we then set out to piece together a complete pathway in *E. coli* for the heterologous expression of Mo-nitrogenase by coexpressing the *nifH,M,Z,D,K,E,N,V* and *fdxN* genes from *A. vinelandii* and the *nifS3,U3,B* genes from *M. acetivorans* in *E. coli* strain MY21.

https://doi.org/10.1038/s41929-024-01229-x

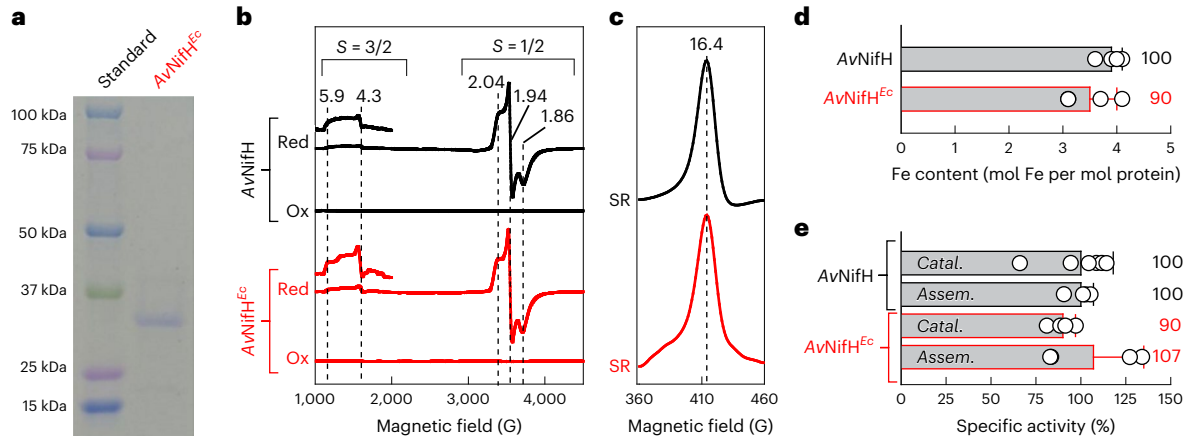

Fig. 3 | Biochemical and spectroscopic analyses of *Av*NifH^{Ec}. **a**, SDS-PAGE of the as-isolated *Av*NifH^{Ec}. Shown is a representative image of three independent experiments with reproducible results. Heterologously expressed in *E. coli* strain YM587EE (Supplementary Table 2), *Av*NifH^{Ec} is a homodimer composed of two ~30 kDa subunits. Standard, Precision Plus Protein Kaleidoscope prestained protein standards (Bio-Rad). **b**,**c**, Perpendicular (**b**) and parallel (**c**) mode EPR spectra of oxidized (Ox), reduced (Red), and super-reduced (SR) states of *Av*NifH^{Ec} (red) compared with those of its native *Av*NifH counterpart (black). The three oxidation states of *Av*NifH^{Ec} or *Av*NifH were generated upon treatment of the protein with IDS (Ox), dithionite (Red) and Eu^{II}-EGTA (SR). The $S = 3/2$ signals observed in the spectra of both reduced *Av*NifH and *Av*NifH^{Ec} are also shown at 5-fold enhanced intensities. **d**, Fe analyses of *Av*NifH and *Av*NifH^{Ec}. The relative Fe content of *Av*NifH^{Ec} (expressed as a percentage) compared with that of *Av*NifH (set as 100%) is indicated in red font. **e**, Activity analyses of *Av*NifH and *Av*NifH^{Ec} in catalysis (Catal.) and M-cluster assembly (Assem.). The relative activities of *Av*NifH^{Ec} (expressed as percentages) compared with those of *Av*NifH (set as 100%) are indicated in red font. See Supplementary Table 4 for details on Fe contents and specific activities. The error bars represent the standard deviation from the mean, originating from four independent Fe analyses (**d**) and four independent M-cluster assembly activity analyses (**e**) of each of *Av*NifH^{Ec} and *Av*NifH, and four and six independent catalytic activity analyses, respectively, of *Av*NifH^{Ec} and *Av*NifH (**e**).

As shown in previous studies, such a system has the gene products required for the successful expression of both components of the *A. vinelandii* Mo-nitrogenase; specifically, this system contains the following components: (1) *Av nifH,M* gene products for the expression of a fully complemented NifH[42]; (2) *Av nifH,M,Z,D,K* gene products for the expression of a P-cluster-replete, yet cofactor-depleted apo NifDK[43]; (3) *Ma nifS3,U3,B* and *Av nifE,N,V* and *fdxN* gene products for the expression of an L-cluster-bound NifEN[43]; (4) *Av nifV* gene product (that is, the homocitrate synthase) for the in vivo synthesis of homocitrate[1], which, along with an in vitro source of molybdenum (that is, molybdate supplemented in the growth medium), should be sufficient to support the maturation of L-cluster on NifEN (the third component above) into an M-cluster via insertion of Mo/homocitrate by NifH (the first component above), followed by transfer of the M-cluster from NifEN to apo NifDK (the second component above) to yield a P-cluster- and M-cluster-replete, holo form of NifDK.

Indeed, when expressed anaerobically in the presence of molybdate, both components of the *A. vinelandii* Mo-nitrogenase could be isolated from the *E. coli* expression strain as soluble, brown proteins. Designated YM587EE and YM538EE, respectively, two *E. coli* expression strains carrying identical biosynthetic components for the expression of a complete, two-component Mo-nitrogenase except for the attachment of a polyhistidine tag to either the reductase component (designated *Av*NifH^{Ec}; YM587EE) or the catalytic component (designated *Av*NifDK^{Ec}; YM538EE) yielded ~60 mg of *Av*NifH^{Ec} and ~30 mg of *Av*NifDK^{Ec}, respectively, per 100 g wet cells. As expected, *Av*NifH^{Ec} is a γ_2-homodimer composed of two ~30 kDa subunits (Fig. 3a). Moreover, *Av*NifH^{Ec} behaves the same way as the native *Av*NifH upon redox conversion, being EPR-silent in the oxidized, $[Fe_4S_4]^{2+}$ state (Fig. 3b, Ox) while displaying mixed $S = 3/2$ ($g = 5.9, 4.3$) and $S = 1/2$ ($g = 2.04, 1.94, 1.86$) EPR signals in the reduced, $[Fe_4S_4]^{+}$ state (Fig. 3b, Red)[1] and a characteristic $g = 16.4$ EPR signal in the super-reduced, $[Fe_4S_4]^{0}$ state (Fig. 3c, SR)[48]. Consistent with a cluster content that is 90% of that of the native *Av*NifH (Fig. 3d), *Av*NifH^{Ec} displays activities in substrate reduction and cluster maturation that are 90% and 107%, respectively, of those of its native counterpart (Fig. 3e).

Likewise, *Av*NifDK^{Ec} closely resembles the native *Av*NifDK in biochemical, spectroscopic and catalytic behaviours. An $\alpha_2\beta_2$-tetramer, *Av*NifDK^{Ec} consists of α- and β-subunits of ~56 kDa and ~59 kDa, respectively (Fig. 4a). Most excitingly, *Av*NifDK^{Ec} exhibits the same M-cluster specific, $S = 3/2$ perpendicular-mode EPR signal at $g = 4.31, 3.67$ and 2.01 in the dithionite-reduced state (Fig. 4b, red trace)[1], as well as the P-cluster (P^{OX}) specific, $g = 11.8$ parallel-mode EPR signal in the indigo disulfonate (IDS)-oxidized state (Fig. 4c, red trace)[49], as its native *Av*NifDK counterpart (Fig. 4b,c, black traces). A comparison of the intensities of the $S = 3/2$ features indicates a 34% occupancy of the M-cluster in *Av*NifDK^{Ec} relative to that in the native *Av*NifDK (Fig. 4b). This assignment aligns well with the activities of N_2-, H^+- and C_2H_2-reduction (38–48%; Fig. 4d) and the molybdenum content (36%; Fig. 5a) of *Av*NifDK^{Ec} relative to those of its native counterpart. Such an alignment of the molybdenum contents, $S = 3/2$ signals and catalytic activities strongly points to the presence of an intact, homocitrate-containing M-cluster in *Av*NifDK^{Ec} like that of its counterpart in the native *Av*NifDK, a suggestion verified by gas chromatography (GC)/gas chromatography–mass spectrometry (GC–MS) analysis of the M-cluster extracted from *Av*NifDK^{Ec} (Fig. 5b,c). Together, these observations firmly establish a content of at least 34% fully active, holo conformation in the as-isolated *Av*NifDK^{Ec}.

Notably, the P-cluster occupancy in *Av*NifDK^{Ec}, assigned as 58% of that in the native *Av*NifDK based on a comparison of the intensities of the P^{OX}-specific, $g = 11.8$ features of the two proteins (Fig. 4c), is much higher than the 34% M-cluster occupancy in *Av*NifDK^{Ec}. Such a discrepancy in P- and M-cluster occupancies suggests the presence of a portion of *Av*NifDK^{Ec} in a P-cluster-replete, but M-cluster-depleted apo conformation, which could be reconstituted and activated by the solvent-extracted M-clusters. In support of this suggestion, upon reconstitution with solvent-extracted M-clusters, *Av*NifDK^{Ec} shows an increase in its C_2H_2-reducing activity to 56% relative to that of its native counterpart (Fig. 4d), which aligns well with the assignment of a 58% P-cluster content in this protein (Fig. 4c). Other than the portion of apo *Av*NifDK^{Ec} that contains the mature P-cluster, there is also a portion of apo *Av*NifDK^{Ec} that contains the P-cluster precursor

https://doi.org/10.1038/s41929-024-01229-x

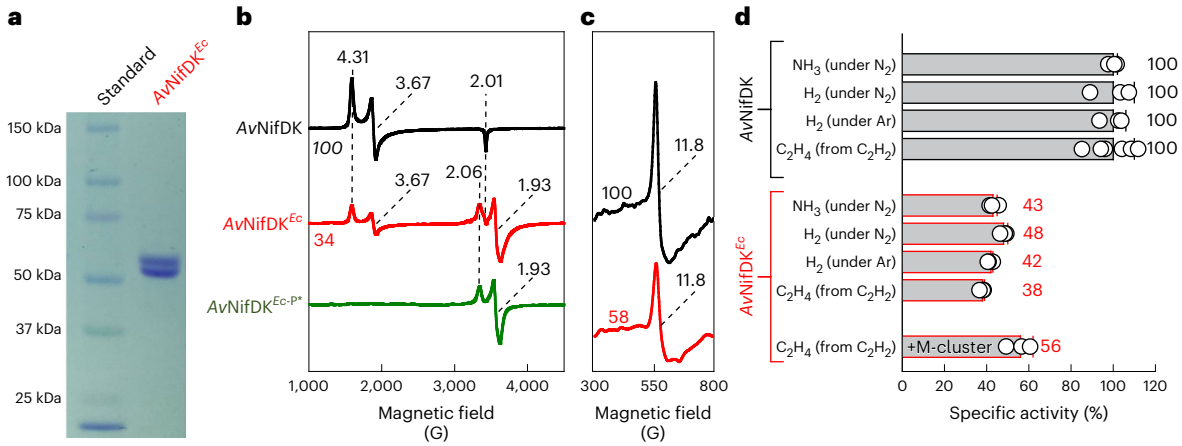

Fig. 4 | Biochemical and spectroscopic analyses of *Av*NifDK^{Ec}. **a**, SDS-PAGE of the as-isolated *Av*NifDK^{Ec}. Shown is a representative image of three independent experiments with reproducible results. Heterologously expressed in *E. coli* strain YM538EE (Supplementary Table 2), *Av*NifDK^{Ec} is a heterotetramer composed of α- and β-subunits of ~56 kDa and ~59 kDa, respectively. Standard, Precision Plus Protein Kaleidoscope prestained protein standards (Bio-Rad). **b**, Perpendicular mode EPR spectra of dithionite-reduced *Av*NifDK, *Av*NifDK^{Ec} and *Av*NifDK$^{Ec\text{-}P^*}$. *Av*NifDK^{Ec} displays an M-cluster specific $S = 3/2$ signal ($g = 4.31, 3.67, 2.01$) identical to that displayed by *Av*NifDK, which integrates to 34% signal intensity of the latter (set as 100%). Additionally, *Av*NifDK^{Ec} displays a P*-cluster (that is, P-cluster precursor) specific $S = 1/2$ signal that is indistinguishable from that displayed by the P*-containing, yet M-cluster-deficient *Av*NifDK$^{Ec\text{-}P^*}$. **c**, Parallel mode EPR spectra of IDS-oxidized *Av*NifDK and *Av*NifDK^{Ec}. *Av*NifDK^{Ec} displays a P-cluster (P^{OX}) specific signal ($g = 11.8$) identical to that displayed by *Av*NifDK, which integrates to 58% signal intensity of the latter (set as 100%). **d**, Activity analyses of *Av*NifH and *Av*NifH^{Ec}. The relative activities of *Av*NifDK^{Ec} (expressed as percentages) compared with those of *Av*NifDK (set as 100%) are indicated in red font. +M-cluster, *Av*NifDK^{Ec} reconstituted with extracted M-clusters. See Supplementary Table 5 for details on specific activities. The error bars represent the standard deviation from the mean, originating from three independent activity analyses of each of *Av*NifDK^{Ec} and *Av*NifDK, except for the C_2H_2-reduction activity analysis of *Av*NifDK that originated from six independent activity analyses (**d**).

(designated P*-cluster), a [Fe_4S_4]-like cluster pair that displays an $S = 1/2$ signal at $g = 2.06$ and 1.93 (Fig. 4b, red) identical to that displayed by the P*-cluster-containing, yet cofactor-deficient apo *Av*NifDK$^{Ec\text{-}P^*}$ (Fig. 4b, green)[43]. The presence of such a species would account for a higher relative Fe content derived from metal analysis (Fig. 5a, Fe (P-site), 68%) than that derived from EPR analysis (Fig. 4c, 58%). Moreover, it could explain the absence of ~44% activity even after reconstitution of *Av*NifDK^{Ec} with the extracted M-clusters (Fig. 4d, +M-cluster).

The presence of cofactor-deficient apo conformations in the as-isolated *Av*NifDK^{Ec} protein is not surprising considering the complexity of nitrogenase assembly and the non-diazotrophic nature of the *E. coli* host that is not optimized for nitrogenase expression. However, despite the coexistence of apo species, the fact that a P-cluster and M-cluster-replete, holo conformation of *Av*NifDK^{Ec} can be isolated at a good yield from *E. coli* and verified for its structural integrity and functional competence is highly important. Given the cluster content and catalytic activity of the holo *Av*NifDK^{Ec} species, the *E. coli* strain YM538EE wherein this *Av*NifDK species is heterologously expressed along with *Av*NifH as a complete nitrogenase should be able to perform in vivo reduction of N_2 to NH_3 and thereby sustain cell growth upon depletion of externally supplied NH_4^+ in the growth medium, a feature that is yet to be conclusively illustrated through a direct measurement of cell mass accumulation and ^{15}N incorporation under nitrogen-fixing conditions.

N_2 reduction by *E. coli* expressing an active Mo-nitrogenase

To examine the in vivo N_2-reducing activity of the *E. coli* strain YM538EE, we initiated cell growth under 100% N_2 or Ar with a limited amount of externally supplied NH_4^+ (2 mM) and monitored the increase of cell density along with the consumption of NH_4^+. Subsequently, we added isopropyl β-D-1-thiogalactopyranoside (IPTG, 0.5 mM) to induce the expression of nitrogenase at ~50% of the maximum cell growth (that is, when ~50% externally supplied NH_4^+ was consumed) and continued to monitor the increase of cell density under 100% N_2 or Ar (Fig. 6a). The strategy of using a limited fixed nitrogen source (that is, NH_4^+) in the starting culture of *E. coli* mimics the so-called de-repression of nitrogenase expression in the native *A. vinelandii* host[1], which permits an initial accumulation of the cell mass of *E. coli* prior to induction while supporting the post-induction synthesis of nitrogenase with the push from the remaining NH_4^+ in the growth medium. As such, upon exhaustion of the remaining NH_4^+, a differentiation of cell growth between cultures grown with (under N_2) and without (under Ar) the substrate of nitrogenase could be accomplished, with the former showing a continued cell growth through nitrogen fixation and the latter incapable of such a feat due to a lack of fixed nitrogen. As predicted, the cell growth of *E. coli* strain YM538EE under N_2 clearly outpaced that under Ar upon addition of IPTG, showing a 26.2% gain in cell density post-induction of nitrogenase expression (Fig. 6b). Given the low energy state of the cells grown under anaerobic conditions, such a post-induction increase in cell density (26%) is not trivial and reflects the diazotrophic contribution from the fraction of holo *Av*NifDK^{Ec} (34%) expressed in the same strain (Figs. 4b–d and 5a).

The in vivo N_2-reducing activity of *E. coli* strain YM538EE was further verified by nanoSIMS experiments, wherein YM538EE was cultivated with a limited amount of NH_4^+ and induced for nitrogenase expression with IPTG under 100% $^{15}N_2$ or Ar using a similar protocol to that used for the growth studies. Subsequently, the $^{15}N_2$- and Ar-treated YM538EE cells were fixed, dried and analysed by a CAMECA nanoSIMS 50L instrument[50]. Excitingly, statistical analyses of secondary ion images derived from nanoSIMS experiments demonstrated a clear difference in ^{15}N isotope enrichment of different samples/controls (Fig. 7a–d; see also Supplementary Figs. 3 and 4). Based on data collected in six different regions of interest (ROIs) of each secondary ion image, the $^{15}N_2$-treated YM538EE (Fig. 7a, 1; Fig. 7b) showed an average $^{15}N/^{14}N$ ratio of 3.1% ± 0.1% that was 8.4-fold higher than the natural abundance $^{15}N/^{14}N$ ratio of 0.37%; in contrast, the Ar-treated YM538EE (Fig. 7a, 2; Fig. 7c) or the $^{15}N_2$-treated, nitrogenase-free *E. coli* strain MY21 (Fig. 7a, 3; Fig. 7d) showed average $^{15}N/^{14}N$ ratios of 0.38% ± 0.01% and 0.41% ± 0.01%, respectively, that were nearly indistinguishable from the natural abundance ^{15}N background. Equivalent to an atom percent

https://doi.org/10.1038/s41929-024-01229-x

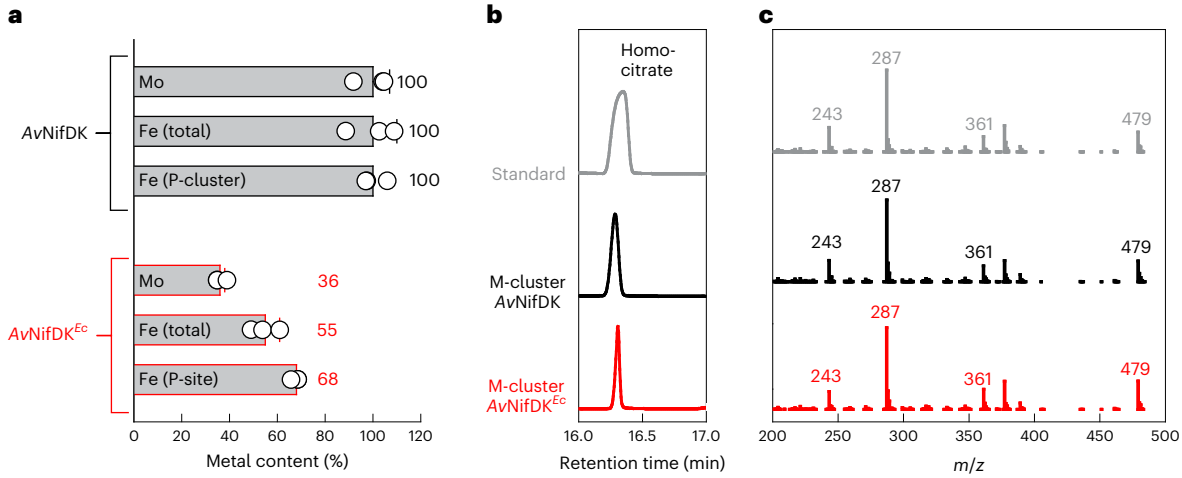

Fig. 5 | Analytical analyses of the metallocentres in *Av*NifDK^{Ec}. **a**, Mo and Fe analyses of *Av*NifDK and *Av*NifDK^{Ec}. The P-cluster content was calculated by subtracting the number of Fe atoms associated with the M-cluster (seven Fe per Mo) from the total number of Fe atoms per NifDK tetramer. Note that the P-cluster site of *Av*NifDK^{Ec} (labelled Fe (P-site)) contains Fe atoms from both P- and P*-clusters. The relative Mo and Fe contents of *Av*NifDK^{Ec} (expressed as percentages) compared with those of *Av*NifDK (set as 100%) are indicated in red font. See Supplementary Table 5 for details on the Fe and Mo contents. The error bars represent the standard deviation from the mean, originating from three independent Fe analyses and three independent Mo analyses of each of *Av*NifDK^{Ec} and *Av*NifDK (**a**). **b**,**c**, GC (**b**) and GC–MS (**c**) chromatography of the homocitrate standard and the homocitrate component in the M-clusters extracted from *Av*NifDK and *Av*NifDK^{Ec}. The *m*/*z* ratios of the derivatized homocitrate fragments used for identifying this organic compound are indicated in the GC–MS fragmentation patterns (**c**).

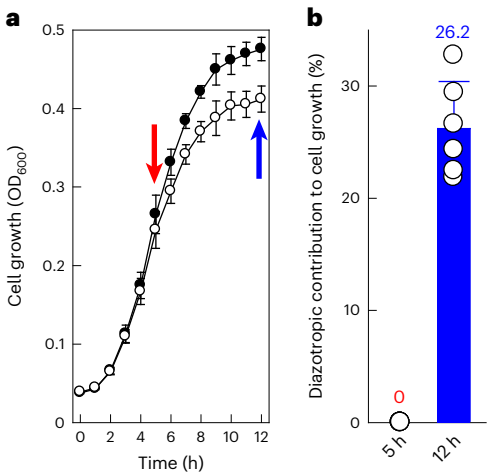

Fig. 6 | Diazotrophic cell growth of the nitrogenase-expressing *E. coli* strain. **a**, Anaerobic cell growth of *E. coli* strain YM538EE in a medium containing a limited amount of ammonia (2 mM) under 100% N_2 (solid circles) or Ar (open circles). Nitrogenase expression was induced at 5 h after inoculation, when the cell growth reached ~50% of the maximum cell density (red arrow), and cell growth was allowed to continue until 12 h after inoculation (blue arrow). The error bars represent the s.e.m., originating from six independent cell growth experiments. **b**, Diazotrophic contribution to the cell growth of YM538EE, showing a 26.2% ± 5.1% gain of cell density 7 h post-induction. Diazotrophic contribution (expressed as a percentage) at the beginning (at 5 h after inoculation) or the end (at 12 h after inoculation) of IPTG induction was calculated by dividing the difference between cell densities under N_2 (**a**, solid circle, at 5 or 12 h) and Ar (**a**, open circle, at 5 or 12 h) by the cell density under Ar (**a**, open circle, at 5 or 12 h). The error bars represent the standard deviation from the mean, originating from six independent experiments.

enrichment of 3% and a net fixation (Fx_{net}) of 5.7% (ref. 51), the 8.4-fold enrichment of ^{15}N in the $^{15}N_2$-grown, YM538EE sample is in stark contrast with the absence of ^{15}N enrichment in the Ar-grown, YM538EE control, which provides conclusive evidence for the in vivo reduction of $^{15}N_2$ by YM538EE and the subsequent incorporation of $^{15}NH_4^+$ into its cellular components. Moreover, the lack of ^{15}N assimilation by the $^{15}N_2$-grown MY21, the nitrogenase-free parent strain of YM538EE, under the same experimental conditions excludes the possibility that the ^{15}N assimilation by YM538EE was caused by ^{15}N contaminants (for example, $^{15}NH_4^+$, $^{15}NO_3^-$) in any component of the nanoSIMS experiments.

The origin of ^{15}N enrichment by YM538EE under nitrogen-fixing conditions can be further correlated with the expression of the oxygen-labile nitrogenase because a stepwise increase in O_2 concentration to 0.1% and 0.2% resulted in a stepwise decrease in ^{15}N enrichment by 29% and 46% (Supplementary Fig. 5). The sensitivity of nitrogenase to O_2, which prevents the nitrogenase-expressing *E. coli* strain YM538EE from being cultivated aerobically, does not present a challenge to *A. vinelandii*. An obligate aerobe, *A. vinelandii* mitigates the problem of O_2 damage of nitrogenase by a number of mechanisms, such as maintaining a high respiration rate during cell growth, forming a slime layer around the cell, and generating an oxygen-protecting complex between Shetna II protein and nitrogenase[52]. The wild-type *A. vinelandii* strain DJ1141 grown aerobically with $^{15}N_2$ displayed an $^{15}N/^{14}N$ ratio of 25.4% ± 1.2%, or a 69-fold ^{15}N enrichment (Fig. 7a,e), approximately eight times higher than that by the *E. coli* strain YM538EE grown anaerobically with $^{15}N_2$ (Fig. 7a,b). Such a discrepancy in ^{15}N assimilation highlights the characteristic of *A. vinelandii* as one of the most robust nitrogen fixers in nature while pointing to the necessity to improve the diazotrophic efficiency of the nitrogenase-expressing *E. coli* strain. Interestingly, under our experimental conditions, the difference between the energy yields of *A. vinelandii* strain DJ1141 (aerobic respiration, 38 ATP/glucose) and *E. coli* strain YM538EE (alcoholic fermentation, 2 ATP/glucose) aligns well with their difference in ^{15}N enrichment, both of which are approximately one order of magnitude. This observation implies that the heterologously expressed nitrogenase could have achieved a much higher diazotrophic efficiency that is comparable to that of its *A. vinelandii* counterpart had it been possible to cultivate the *E. coli* expression strain under aerobic conditions for an enhanced energy yield. As such, the development of strategies that address the oxygen sensitivity of nitrogenase concomitant with enhanced cellular energetics appears to be the logical next step to improve our prototype *E. coli* expression system.

Although our prototype *E. coli* expression system is much less efficient than its *A. vinelandii* counterpart in performing diazotrophy,

https://doi.org/10.1038/s41929-024-01229-x

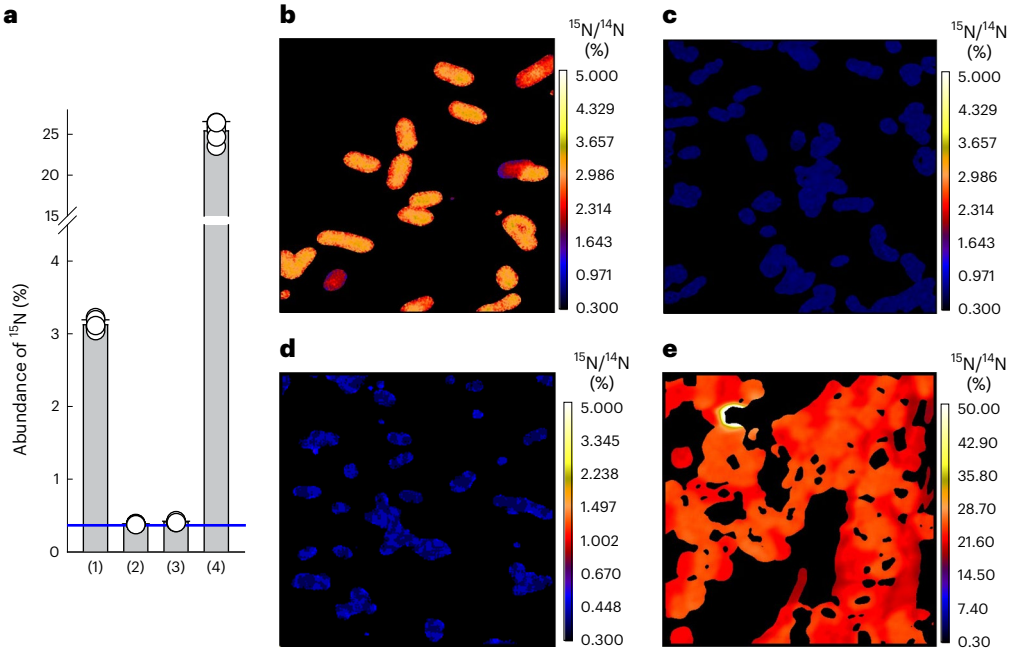

Fig. 7 | Diazotrophic nitrogen assimilation by the nitrogenase-expressing *E. coli* strain. a, Statistical analysis of secondary ion images derived from nanoSIMS experiments (**b**–**e**): (1) *E. coli* strain YM538EE expressing nitrogenase in the presence of 100% $^{15}N_2$ (**b**); (2) *E. coli* strain YM538EE expressing nitrogenase in the presence of 100% Ar (**c**); (3) *E. coli* strain MY21 grown in the presence of 100% $^{15}N_2$ (**d**); and (4) *A. vinelandii* strain DJ1141 grown in the presence of 100% $^{15}N_2$ (**e**). The *A. vinelandii* strain DJ1141 was grown aerobically with a limited amount of ammonia in the medium, followed by derepression, or up-regulation of nitrogenase expression, for 3 h upon exhaustion of ammonia. The ^{15}N abundance of each sample or control (**a**) was calculated based on data collected in six different ROIs of the corresponding nanoSIMS image (**b**–**e**). The average values of ^{15}N abundance (or ^{15}N/^{14}N), expressed as the standard deviation of the mean of six different ROIs of each sample or control, are as follows: (1) 3.1% ± 0.1%, (2) 0.38% ± 0.01%, (3) 0.41% ± 0.01% and (4) 25.4% ± 1.2%. Given the natural ^{15}N abundance, or ^{15}N/^{14}N of 0.37% (indicated by a blue line in **a**), the level of ^{15}N enrichment for each sample can be calculated as follows: (1) 8.4-fold, (2) 1.03-fold, (3) 1.11-fold and (4) 69-fold. For (1), the ^{15}N enrichment can also be expressed as an atom percent enrichment of 3% and a net fixation (Fx_{net}) of 5.7% (ref. 51); additionally, a normalized ^{15}N abundance of 11.8% ± 0.4% can be calculated solely based on the post-induction gain of cell density by 26% (Fig. 6b). The quality check of the $^{15}N_2$ source is shown in Supplementary Fig. 3. The nanoSIMS experiments were conducted on seven independent samples of *E. coli* strain YM538EE expressing nitrogenase under 100% $^{15}N_2$ and four independent controls of *E. coli* strain MY21 grown under 100% $^{15}N_2$. Representative results of the samples and the controls are shown in this figure, and the statistical analyses of six additional samples and three additional controls are shown in Supplementary Fig. 4.

the fact that a non-diazotrophic host such as *E. coli* can clearly acquire a nitrogen-fixing ability strongly points to the feasibility of transgenic expression of nitrogenase while suggesting the possibility of tweaking the system towards utility. To test this concept, we deleted *amtB*, the gene encoding the ammonia transporter protein AmtB[53], in the genome of YM538EE. Inhibited at higher ammonium concentrations where cells take up ammonia via passive diffusion, AmtB serves to scavenge low concentrations of ammonium (<1 mM) from the environment[54]. Thus, the YM538EE-derived, *amtB*-deletion strain (designated YM559EE) could still take up externally supplied ammonia (2 mM) via passive diffusion for the initial cell mass accumulation and post-induction nitrogenase expression; yet, it would become leaky and permit accumulation of extracellular ammonia due to a lack of AmtB-dependent reuptake of low concentrations of the new ammonia that is generated through nitrogen fixation and subsequently released into the medium. Indeed, frequency-selective NMR analysis[55] of the supernatant collected after centrifugation of the YM559EE culture, which was first grown with limited $^{14}NH_4^+$ and then induced for nitrogenase expression under $^{15}N_2$, revealed an accumulation of extracellular $^{15}NH_4^+$ (as reflected by the doublet at 6.99 and 7.12 ppm) that originated from the reduction of $^{15}N_2$ by the heterologously expressed nitrogenase (Fig. 8a). Incubation of the supernatant of the $^{15}N_2$-grown YM559EE culture with the nitrogenase-free *E. coli* strain MY21 resulted in a 4.3-fold ^{15}N enrichment (Fig. 8b,c) that was not observed in the control experiment conducted with the supernatant of the $^{14}N_2$-grown YM559EE culture (Fig. 8b,d). This observation not only provides further verification of the heterologously expressed nitrogenase as the origin of ^{15}N enrichment in a non-diazotrophic organism, but also suggests the utility of our heterologous expression system as a potential template for the biotechnological adaptation of nitrogenase-based applications.

Conclusions

In this work, we successfully expressed an active *A. vinelandii* Mo-nitrogenase in *E. coli* by transferring an essential minimum set of *nif* genes into this non-diazotrophic host. The biochemical and spectroscopic analyses conclusively verified the heterologous synthesis of the crucial metallocentres in the heterologously expressed nitrogenase; whereas the growth, nanoSIMS and NMR experiments clearly demonstrated the ability of the developed nitrogenase-expressing *E. coli* strain to sustain diazotrophic cell growth upon exhaustion of ammonia as well as accumulate extracellular ammonia upon deletion of *amtB*. The presence of immature, apo species in the as-isolated *Av*NifDK component of the heterologously expressed nitrogenase, and the unfavourable fermentation conditions that restrict the physiological function of this enzyme, clearly point to a need to further optimize this system with respect to the assembly components and/or the host system. Yet, the in vitro and in vivo N_2-reducing activities reported herein, coupled with the conclusive demonstration of the heterologous formation of complex metallocentres in the purified nitrogenase proteins, provide an unambiguous read-out for further evolving this system into one that is fully competent in performing diazotrophy without the extra push provided by any externally supplied ammonia. Given the genetically amenable characteristic of the *E. coli* host, it is conceivable that such a system could be readily modified—as exemplified by the construction

https://doi.org/10.1038/s41929-024-01229-x

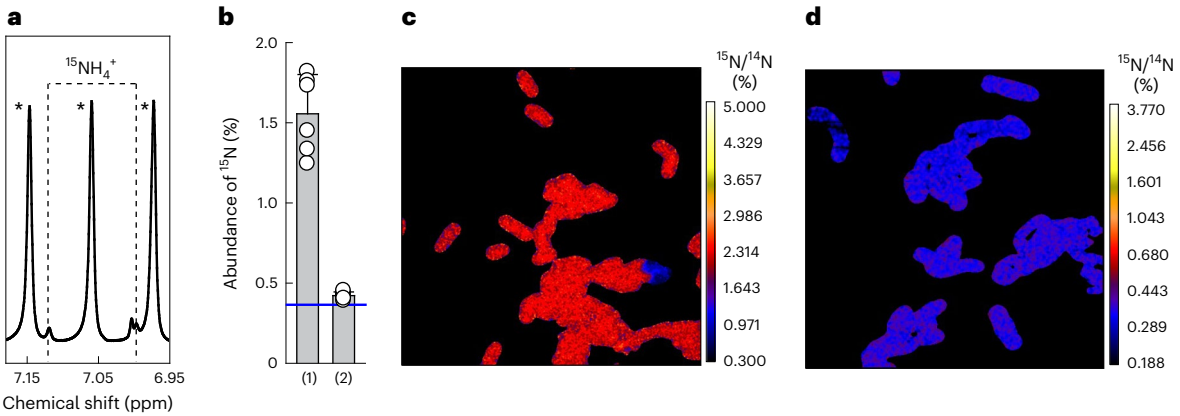

Fig. 8 | Ammonia excretion by *E. coli* strain expressing a functional nitrogenase. a, Frequency-selective pulse ^{1}H NMR spectrum of $^{15}NH_4^+$ excreted by *E. coli* strain YM559EE expressing nitrogenase in the presence of 100% $^{15}N_2$ the same way as described for *E. coli* strain YM538EE in Fig. 6a. See Supplementary Table 2 for strain construction. Ammonia excretion was quantified as ~2.5 mmol NH_4^+ per gramme of cells. The symbol * indicates the $^{14}NH_4^+$-specific triplet signal. **b**, Statistical analysis of secondary ion images derived from nanoSIMS experiments (**c**,**d**), wherein *E. coli* strain MY21 was grown with NH_4^+ excreted by *E. coli* strain YM559EE in the presence of (1) $^{15}N_2$ (**c**) and (2) $^{14}N_2$ (**d**). The nanoSIMS experiments (**c**,**d**) were each conducted on one sample. The ^{15}N abundance of each sample (**b**) was calculated based on data collected in six different ROIs of the corresponding nanoSIMS image (**c**,**d**). The average values of ^{15}N abundance (or $^{15}N/^{14}N$), expressed as the standard deviation of the mean of six different ROIs of each sample or control, are as follows: (1) 1.6% ± 0.3% and (2) 0.42% ± 0.02%. Given the natural ^{15}N abundance, or $^{15}N/^{14}N$ of 0.37% (indicated by a blue line in **b**), the level of ^{15}N enrichment for each sample can be calculated as follows: (1) 4.3-fold and (2) 1.14-fold.

of a leaky strain for the extracellular accumulation of ammonia—for future biotechnological adaptations of nitrogenase-based applications. Moreover, the *E. coli* expression system described in this work can be used as a simple, yet useful model for deducing principles of optimizing the efficiency of nitrogen fixation in a non-diazotrophic organism, which could facilitate future efforts toward generating autonomous N_2-fixing systems in higher organisms, such as plants, via transgenic expression of nitrogenase.

Methods

All chemicals were purchased from Sigma-Aldrich and Thermo Fisher Scientific unless specified otherwise. All experiments were conducted in a glovebox or on a Schlenk line under an Ar atmosphere, with an O_2 concentration of <3 ppm. The experimental details are provided below or in the Supplementary Information.

Strain construction

For the heterologous synthesis of an L-cluster-bound NifEN, the genes encoding the *A. vinelandii* NifE (with an N-terminal polyhistidine tag), NifN and the *M. acetivorans* NifS3, NifU3 and NifB proteins were codon-optimized for *E. coli* expression, synthesized and cloned into pCDFDuet-1 (GenScript) as summarized in Supplementary Table 2. Subsequently, these constructs were transformed into *E. coli* strain MY21, which was derived from *E. coli* strain BL21(DE3) but contained a deletion of *iscR*, the gene encoding a transcription repressor for the *isc* operon, in the genome (GenScript). This procedure resulted in an *E. coli* strain (strain YM577EE) expressing a His-tagged, L-cluster-bound *Av*NifEN^{Ec} upon induction with IPTG. The deletion of *iscR* in *E. coli* has been shown to greatly improve the FeS maturation and expression yield of the heterologously synthesized [FeFe] hydrogenase[56,57]. This effect could be attributed to a substantially upregulated expression of the FeS machinery in the *E. coli* host, which not only satisfies the need of the host to synthesize its own FeS proteins, but also benefits the overexpression of the foreign FeS enzymes by directly supplying FeS units for their maturation and/or indirectly reducing the competition for FeS sources from the host FeS-biosynthetic events.

For the heterologous synthesis of a complete Mo-nitrogenase, the genes encoding the *A. vinelandii* NifH (with or without an N-terminal polyhistidine tag), NifM, NifZ, NifD (with or without an N-terminal polyhistidine tag or a C-terminal streptavidin tag), NifK, NifE, NifN, NifV and FdxN proteins and the *M. acetivorans* NifS3, NifU3 and NifB proteins were codon-optimized for *E. coli* expression, synthesized and cloned into pCDFDuet-1 or pRSFDuet-1 (GenScript) as summarized in Supplementary Table 2. Subsequently, these constructs were transformed into *E. coli* strain MY21. This procedure resulted in *E. coli* strains expressing the Mo-nitrogenase of *A. vinelandii* comprising either a non-tagged *Av*NifH^{Ec} and a His/Strep-tagged *Av*NifDK^{Ec} (strain YM538EE) or a His-tagged *Av*NifH^{Ec} and a non-tagged *Av*NifDK^{Ec} (strain YM587EE) upon induction with IPTG, in the presence of molybdate supplied in the medium. In addition, the previously reported *E. coli* strain YM387EE[43], which carries genes encoding the *A. vinelandii* NifZ, NifD and NifK proteins for the heterologous expression of a His-tagged, P*-cluster (P*, P-cluster precursor; 2x[Fe_4S_4]) containing, yet cofactor-deficient *Av*NifDK species (designated *Av*NifDK$^{Ec\text{-}P^*}$), was used for the comparative analysis with YM538EE.

For the creation of a leaky strain capable of accumulating extracellular ammonia, the plasmids used for the construction of YM538EE (see above) were transformed into *E. coli* strain MY23, which was derived from *E. coli* strain BL21(DE3) but contained a deletion of *iscR* along with a deletion of *amtB*, the gene encoding the ammonia transporter protein AmtB, in the genome (GenScript). This procedure resulted in an *E. coli* strain (strain YM559EE; Supplementary Table 2) expressing the Mo-nitrogenase of *A. vinelandii* upon induction with IPTG and capable of accumulating ammonia in the medium due to the deletion of AmtB.

Cell growth and protein purification

E. coli strains YM538EE, YM577EE, YM559EE and YM387EE, were grown in 10 l batches in LB medium (Difco) supplemented with 50 mM MOPS/NaOH (pH 7.4), 25 mM glucose, 2 mM ferric ammonium citrate, 19 mg l^{-1} kanamycin and 26 mg l^{-1} streptomycin in a BIOFLO 415 fermenter (New Brunswick Scientific) at 37 °C with 200 rpm agitation and 10 l min^{-1} airflow. When OD_{600} reached 0.5, the airflow was terminated and the fermenter was purged with N_2 (ultrahigh purity) at a rate of 1.5 l min^{-1}; additionally, the temperature was lowered to 24 °C. Once the culture reached 24 °C, 2 mM cysteine was added and the expression of nitrogenase was induced by the addition of 250 µM IPTG. Protein expression was allowed to continue for 16 h prior to harvesting of the cells by centrifugation using a Thermo Fisher Scientific Legend XTR centrifuge.

The heterologously expressed His-tagged *Av*NifEN^{Ec}, His-tagged *Av*NifH^{Ec}, His/Strep-tagged *Av*NifDK^{Ec} and His-tagged *Av*NifDK$^{Ec\text{-}P^*}$ proteins were purified by immobilized metal affinity chromatography using a method adapted from the purification of the His-tagged nitrogenase proteins from *A. vinelandii*[26,34]. Following immobilized metal affinity chromatography with Ni Sepharose (Cytiva), the His/Strep-tagged *Av*NifDK^{Ec}-containing fraction that eluted at 40 mM imidazole was further purified by Strep-tag affinity chromatography in a glovebox filled with Ar. The protein was loaded on a column packed with PureCube HiCap Streptactin Agarose XL (Cube Biotech) in a buffer containing 100 mM Tris–HCl (pH 8.0), 150 mM NaCl and 2 mM dithiothreitol (DTT), followed by washing of the column with 5 column volumes of the loading buffer and elution of the protein using the same buffer that contained an additional 2.5 mM desthiobiotin. The eluted protein was then concentrated using an Amicon Ultra centrifugal filter with a molecular weight cut-off of 100 kDa (Sigma) at 7,000 rpm for 25 min at 10 °C, followed by addition of sodium dithionite ($Na_2S_2O_4$) to the concentrated protein at a final concentration of 5 mM and storage of the frozen protein sample in liquid N_2.

A. vinelandii strains DJ1162, DJ1141, DJ1143 and DJ1041 expressing His-tagged *Av*NifH, *Av*NifDK and *Av*NifEN, respectively[26,34], were grown in 180 l batches in Burke's minimal medium (supplemented with 2 mM ammonium acetate)[58] in a 200 l fermenter (New Brunswick Scientific) at 30 °C with 100 rpm agitation and 30 l min^{-1} airflow. Cell growth was monitored at OD_{436} using a Spectronic 20 Genesys spectrometer (Spectronic Instruments). Upon depletion of ammonia, cells were de-repressed for 3 h prior to being harvested by a flow-through centrifugal harvester (Cepa). Published methods were used to purify His-tagged *Av*NifH, *Av*NifDK and *Av*NifEN[26,34]. Note that *Av*NifDK^{P} is cofactor-deficient but contains a P-cluster (*Av*NifDK^{P}, $[Fe_8S_7]$); whereas *Av*NifEN contains an O-cluster ($[Fe_4S_4]$) and an L-cluster ($[Fe_8S_9C]$).

Metal and homocitrate analyses

The metal contents of *Av*NifEN, *Av*NifEN^{Ec}, *Av*NifH, *Av*NifH^{Ec}, *Av*NifDK and *Av*NifDK^{Ec} were determined by inductively coupled plasma optical emission spectroscopy using an iCAP7000 spectrometer (Thermo Scientific Scientific). Calibration of the equipment was performed by using standard solutions made via dilution of stock solutions of elemental iron (1 mg ml^{-1}) and molybdenum (0.1 mg ml^{-1}), respectively. The protein sample was first mixed with 100 µl of concentrated sulfuric acid (H_2SO_4) and 100 µl of concentrated nitric acid (HNO_3) and subsequently heated for 30 min at 250 °C. Such a procedure was repeated until the solution became colourless, followed by cooling of the solution to room temperature and dilution of the solution to a total volume of 10 ml with 2% HNO_3 prior to metal analysis. Homocitrate in the M-cluster extracted from *Av*NifDK^{Ec} was analysed as described previously[59,60].

Substrate reduction assays

The C_2H_2- and N_2-reduction assays were performed at 30 °C in 9.5 ml vials fitted with rubber serum stoppers and metal caps (DWK Life Science), which contained 0.1 atm C_2H_2/0.9 atm Ar for the C_2H_2-reduction assays involving *Av*NifDK^{Ec} and *Av*NifH^{Ec}, 0.6 atm C_2H_2/0.4 atm Ar for the C_2H_2-reduction assay involving *Av*NifEN^{Ec}, or 1.0 atm N_2 for the N_2-reduction assays involving *Av*NifDK^{Ec} and *Av*NifH^{Ec}.

The reaction that tested the activity of *Av*NifDK^{Ec} or *Av*NifH^{Ec} contained, in a total volume of 1 ml, 25 mM Tris-HCl (pH 8.0), 2.5 mM ATP, 5.0 mM $MgC1_2$, 30 mM creatine phosphate, 0.125 mg of creatine phosphokinase and 20 mM $Na_2S_2O_4$; whereas the reaction that tested the activity of *Av*NifEN^{Ec} had the same composition except for a lower concentration of $Na_2S_2O_4$ at 0.5 mM. The assay testing the activity of *Av*NifDK^{Ec} was initiated by the addition of 0.15 mg *Av*NifDK^{Ec} and 1.25 mg of *Av*NifH; the assay testing the activity of *Av*NifH^{Ec} was initiated by the addition of 2.4 mg of *Av*NifDK and 0.36 mg of *Av*NifH^{Ec}; and the assay testing the activity of *Av*NifEN^{Ec} was initiated by the addition of 0.15 mg of *Av*NifEN^{Ec} and 1.75 mg of *Av*NifH. Subsequently, all assays were incubated at 30 °C for 10 min, quenched with EDTA, and analysed for product formation.

To detect C_2H_4 as a product of C_2H_2 reduction, 250 µl of the headspace was injected into a GC flame ionization device (SRI Instruments) equipped with a packed Poropak N column (Restek). Calibration was achieved by injecting 15 ppm C_2H_4 gas standard under the same conditions. To detect NH_3 as the product of N_2 reduction, 100 µl of the reaction was added to an *o*-phthalaldehyde solution that contained, in a total volume of 1 ml, 10 mM *o*-phthalaldehyde and 2.5 mM 2-mercaptomethanol in a 50 mM potassium phosphate buffer (pH 7.8). The mixture was allowed to sit at room temperature for 3 h, followed by measurement using a fluorescence spectrophotometer (RF-5301PC, Shimadzu) with the excitation wavelength set at 361 nm and the emission wavelength set at 423 nm.

M-cluster maturation assays

Each assay contained, in a total volume of 0.9 ml, 25 mM Tris-HCl (pH 8.0), 0.4 mM homocitrate, 0.4 mM Na_2MoO_4, 2.4 mM ATP, 4.8 mM $MgCl_2$, 30 mM creatine phosphate, 24 units of creatine phosphokinase, 20 mM $Na_2S_2O_4$, 0.45 mg of *Av*NifDK^{P} (isolated from *A. vinelandii* strain DJ1143; ref. 26) and either 1.2 mg of *Av*NifH^{Ec} (isolated from *E. coli* strain YM587EE) plus 1.0 mg *Av*NifEN (isolated from *A. vinelandii* strain DJ1041; ref. 34), or 1.2 mg of *Av*NifH plus 1.0 mg of *Av*NifEN^{Ec} (isolated from *E. coli* strain YM577EE). The assay was incubated at 30 °C for 60 min and subsequently split into triplicates in three 9.5 ml vials. Each vial contained, in a total volume of 0.7 ml, 25 mM Tris-HCl (pH 8.0), 2.5 mM ATP, 5.0 mM $MgCl_2$, 30 mM creatine phosphate, 0.125 mg of creatine phosphokinase, 20 mM $Na_2S_2O_4$, 1.05 mg of *Av*NifH and 0.1 atm C_2H_2/0.9 atm Ar in the headspace. The mixture was then incubated at 30 °C for 10 min and analysed for product formation as described above.

M-cluster reconstitution assays

Each assay contained, in a total volume of 0.9 ml, 25 mM Tris-HCl (pH 8.0), 20 mM $Na_2S_2O_4$, 0.45 mg of *Av*NifDK^{P} or *Av*NifDK^{Ec}, and 6 ml of isolated M-clusters[61]. The assay was incubated at 30 °C for 15 min and subsequently split into triplicates in three 9.5 ml vials. Each vial contained, in a total volume of 0.7 ml, 25 mM Tris-HCl (pH 8.0), 2.5 mM ATP, 5.0 mM $MgCl_2$, 30 mM creatine phosphate, 0.125 mg of creatine phosphokinase, 20 mM $Na_2S_2O_4$, 1.05 mg of *Av*NifH and 0.1 atm C_2H_2/0.9 atm Ar in the headspace. The mixture was then incubated at 30 °C for 10 min and analysed for product formation as described above.

EPR experiments

EPR samples were prepared in a Vacuum Atmospheres glovebox filled with Ar and operated at <3 ppm O_2, and flash frozen in liquid nitrogen prior to analysis. The reduced samples contained 25 mM Tris-HCl (pH 8.0), 10% (vol/vol) glycerol, 250 mM imidazole and 2 mM $Na_2S_2O_4$; the oxidized samples were prepared by incubating the reduced samples with excess indigo disulfonate (IDS); and the super-reduced samples were prepared by adding excess europium(II) ethylene glycol-bis(β-aminoethyl ether)-*N*,*N*,*N*,*N*-tetraacetic acid (Eu^{II}-EGTA). The concentrations of the reduced and oxidized NifH and NifDK samples were 15 mg ml^{-1}; the concentration of the oxidized NifEN samples was 15 mg ml^{-1}; and the concentrations of the oxidized NifDK and the super-reduced NifH samples were 8 mg ml^{-1}. The NifH, NifDK and NifEN samples refer to those isolated from either *A. vinelandii* or *E. coli*.

EPR data were acquired through an ESP 300E spectrophotometer (Bruker) interfaced with an ESR-9002 liquid-helium continuous-flow cryostat (Oxford Instruments) using a microwave power of 5 mW, a gain of 5×10^4, a modulation frequency of 100 kHz and a modulation amplitude of 5 G. Five scans of perpendicular-mode EPR spectra were recorded for each sample at 10 K (reduced NifH or NifDK) or 15 K (oxidized NifH or NifEN) using a microwave frequency of 9.62 GHz; and eight scans of parallel-mode EPR spectra were recorded for each

sample at 10 K (super-reduced NifH or oxidized NifDK) using a microwave frequency of 9.38 GHz. EasySpin 5.2.27 toolbox was used for EPR data analysis.

Cell growth experiments

A 10 ml culture of *E. coli* strain YM538EE was grown in LB medium (Difco) supplemented with 19 mg l^{-1} kanamycin and 26 mg l^{-1} streptomycin in a 50 ml conical tube at 37 °C with 200 rpm agitation overnight. Subsequently, 1 ml aliquots of the overnight culture were transferred to 1.5 ml microtubes and centrifuged at 10,000 rpm for 4 min, followed by careful removal of the supernatant. Each cell pellet was then washed with double-distilled H_2O and subsequently resuspended in 1 ml of supplemented M9 medium containing 0.4% glucose, 2 mM $MgSO_4$, 0.1 mM $CaCl_2$, 12.8 mg ml^{-1} Na_2HPO_4, 3 mg ml^{-1} KH_2PO_4, 0.5 mg ml^{-1} NaCl, 2 mM NH_4Cl, 0.024 mg ml^{-1} Na_2MoO_4, 0.054 mg ml^{-1} $FeCl_3$ and 1 mM cysteine. The cells derived from each resuspended pellet were inoculated into a 250 ml screw-capped flask with a septum-sealed side-arm containing 100 ml of the supplemented M9 medium, 19 mg l^{-1} kanamycin and 26 mg l^{-1} streptomycin. The gas atmospheres of the flasks were then exchanged with either 100% Ar or 100% N_2 by sparging under the respective gases for 5 min. The flasks were then vented carefully via the screw cap to remove excess pressure.

The cultures were grown anaerobically at 37 °C with 200 rpm agitation, with 1 ml of each culture removed at 1 h time intervals via the side-arm septum with a sterile syringe for the measurement of cell density at OD_{600} and the concurrent determination of ammonia consumption in the medium. After 5 h, the cell growth reached ~50% of the expected maximum cell density (determined on the basis of control experiments with uninduced YM538EE), which corresponded to a consumption of ~50% of the externally supplied ammonia. At this point, the cultures were induced by addition of 0.1 ml of a 500 mM IPTG stock via the side-arm septum using a sterile syringe, followed by removal of 1 ml of each culture at 1 h time intervals until 12 h post-inoculation. The 1 ml culture taken at each time point was first determined for cell density at OD_{600} and then transferred to a 1.5 ml microtube. Following centrifugation of the 1 ml culture at 13,000 rpm for 5 min, 0.5 ml of the supernatant was carefully removed and transferred to a new 1.5 ml microtube. The supernatants collected throughout the cell growth (pre- and post-induction) were stored at −20 °C until the ammonia concentrations for all samples were determined as described above.

Reporting summary

Further information on research design is available in the Nature Portfolio Reporting Summary linked to this article.

Data availability

All data are available from the authors upon reasonable request. Source data are provided with this paper.

References

1. Burgess, B. K. & Lowe, D. J. Mechanism of molybdenum nitrogenase. *Chem. Rev.* **96**, 2983–3012 (1996).
2. Hu, Y. et al. Enzymatic Fischer–Tropsch-type reactions. *Chem. Rev.* **123**, 5755–5797 (2023).
3. Jasniewski, A. J., Lee, C. C., Ribbe, M. W. & Hu, Y. Reactivity, mechanism, and assembly of the alternative nitrogenases. *Chem. Rev.* **120**, 5107–5157 (2020).
4. Lee, C. C., Hu, Y. & Ribbe, M. W. Catalytic reduction of CN^-, CO, and CO_2 by nitrogenase cofactors in lanthanide-driven reactions. *Angew. Chem. Int. Ed.* **54**, 1219–1222 (2015).
5. Lee, C. C., Hu, Y. & Ribbe, M. W. Vanadium nitrogenase reduces CO. *Science* **329**, 642 (2010).
6. Lee, C. C., Hu, Y. & Ribbe, M. W. Tracing the hydrogen source of hydrocarbons formed by vanadium nitrogenase. *Angew. Chem. Int. Ed.* **50**, 5545–5547 (2011).
7. Rofer-DePoorter, C. K. A comprehensive mechanism for the Fischer–Tropsch synthesis. *Chem. Rev.* **81**, 447–474 (1981).
8. Rommens, K. T. & Saeys, M. Molecular views on Fischer–Tropsch synthesis. *Chem. Rev.* **123**, 5798–5858 (2023).
9. Smith, C., Hill, A. K. & Torrente-Murciano, L. Current and future role of Haber–Bosch ammonia in a carbon-free energy landscape. *Energy Environ. Sci.* **13**, 331–344 (2020).
10. Erisman, J. W., Sutton, M. A., Galloway, J., Klimont, Z. & Winiwarter, W. How a century of ammonia synthesis changed the world. *Nat. Geosci.* **1**, 636–639 (2008).
11. Rutledge, H. L. & Tezcan, F. A. Electron transfer in nitrogenase. *Chem. Rev.* **120**, 5158–5193 (2020).
12. Stripp, S. T. et al. Second and outer coordination sphere effects in nitrogenase, hydrogenase, formate dehydrogenase, and CO dehydrogenase. *Chem. Rev.* **122**, 11900–11973 (2022).
13. Rutledge, H. L., Cook, B. D., Nguyen, H. P. M., Herzik, M. A. Jr & Tezcan, F. A. Structures of the nitrogenase complex prepared under catalytic turnover conditions. *Science* **377**, 865–869 (2022).
14. Schindelin, H., Kisker, C., Schlessman, J. L., Howard, J. B. & Rees, D. C. Structure of ADP·AlF_4^--stabilized nitrogenase complex and its implications for signal transduction. *Nature* **387**, 370–376 (1997).
15. Spatzal, T. et al. Evidence for interstitial carbon in nitrogenase FeMo cofactor. *Science* **334**, 940 (2011).
16. Lancaster, K. M. et al. X-ray emission spectroscopy evidences a central carbon in the nitrogenase iron–molybdenum cofactor. *Science* **334**, 974–977 (2011).
17. Wiig, J. A., Hu, Y., Lee, C. C. & Ribbe, M. W. Radical SAM-dependent carbon insertion into the nitrogenase M-cluster. *Science* **337**, 1672–1675 (2012).
18. Hu, Y. & Ribbe, M. W. Biosynthesis of the metalloclusters of nitrogenases. *Annu. Rev. Biochem.* **85**, 455–483 (2016).
19. Hu, Y. & Ribbe, M. W. Biosynthesis of the metalloclusters of molybdenum nitrogenase. *Microbiol. Mol. Biol. Rev.* **75**, 664–677 (2011).
20. Hu, Y. & Ribbe, M. W. Biosynthesis of the iron–molybdenum cofactor of nitrogenase. *J. Biol. Chem.* **288**, 13173–13177 (2013).
21. Corbett, M. C. et al. Comparison of iron–molybdenum cofactor-deficient nitrogenase MoFe proteins by X-ray absorption spectroscopy: implications for P-cluster biosynthesis. *J. Biol. Chem.* **279**, 28276–28282 (2004).
22. Lee, C. C. et al. Stepwise formation of P-cluster in nitrogenase MoFe protein. *Proc. Natl Acad. Sci. USA* **106**, 18474–18478 (2009).
23. Schmid, B. et al. Structure of a cofactor-deficient nitrogenase MoFe protein. *Science* **296**, 352–356 (2002).
24. Rupnik, K., Lee, C. C., Hu, Y., Ribbe, M. W. & Hales, B. J. A VTVH MCD and EPR spectroscopic study of the maturation of the 'second' nitrogenase P-cluster. *Inorg. Chem.* **57**, 4719–4725 (2018).
25. Hu, Y., Fay, A. W., Lee, C. C. & Ribbe, M. W. P-cluster maturation on nitrogenase MoFe protein. *Proc. Natl Acad. Sci. USA* **104**, 10424–10429 (2007).
26. Hu, Y., Fay, A. W., Dos Santos, P. C., Naderi, F. & Ribbe, M. W. Characterization of *Azotobacter vinelandii nifZ* deletion strains. Indication of stepwise MoFe protein assembly. *J. Biol. Chem.* **279**, 54963–54971 (2004).
27. Liu, Y. A. et al. Radical SAM-dependent formation of a nitrogenase cofactor core on NifB. *J. Inorg. Biochem.* **233**, 111837 (2022).
28. Fay, A. W., Wiig, J. A., Lee, C. C. & Hu, Y. Identification and characterization of functional homologs of nitrogenase cofactor biosynthesis protein NifB from methanogens. *Proc. Natl Acad. Sci. USA* **112**, 14829–14833 (2015).
29. Rettberg, L. A. et al. Probing the coordination and function of Fe_4S_4 modules in nitrogenase assembly protein NifB. *Nat. Commun.* **9**, 2824 (2018).

30. Jasniewski, A. J. et al. Spectroscopic characterization of an eight-iron nitrogenase cofactor precursor that lacks the '9th sulfur'. *Angew. Chem. Int. Ed.* **58**, 14703–14707 (2019).
31. Tanifuji, K. et al. Tracing the 'ninth sulfur' of the nitrogenase cofactor via a semi-synthetic approach. *Nat. Chem.* **10**, 568–572 (2018).
32. Tanifuji, K. et al. Tracing the incorporation of the 'ninth sulfur' into the nitrogenase cofactor precursor with selenite and tellurite. *Nat. Chem.* **13**, 1228–1234 (2021).
33. Kang, W. et al. X-ray crystallographic analysis of NifB with a full complement of clusters: structural insights into the radical SAM-dependent carbide insertion during nitrogenase cofactor assembly. *Angew. Chem. Int. Ed.* **60**, 2364–2370 (2021).
34. Hu, Y., Fay, A. W. & Ribbe, M. W. Identification of a nitrogenase FeMo cofactor precursor on NifEN complex. *Proc. Natl Acad. Sci. USA* **102**, 3236–3241 (2005).
35. Corbett, M. C. et al. Structural insights into a protein-bound iron–molybdenum cofactor precursor. *Proc. Natl Acad. Sci. USA* **103**, 1238–1243 (2006).
36. Kaiser, J. T., Hu, Y., Wiig, J. A., Rees, D. C. & Ribbe, M. W. Structure of precursor-bound NifEN: a nitrogenase FeMo cofactor maturase/insertase. *Science* **331**, 91–94 (2011).
37. Hu, Y. et al. FeMo cofactor maturation on NifEN. *Proc. Natl Acad. Sci. USA* **103**, 17119–17124 (2006).
38. Hu, Y. et al. Nitrogenase Fe protein: a molybdate/homocitrate insertase. *Proc. Natl Acad. Sci. USA* **103**, 17125–17130 (2006).
39. Yoshizawa, J. M. et al. Optimization of FeMoco maturation on NifEN. *J. Am. Chem. Soc.* **131**, 9321–9325 (2009).
40. Stiebritz, M. T. et al. Ambient conversion of CO_2 to hydrocarbons by biogenic and synthetic $[Fe_4S_4]$ clusters. *Nat. Catal.* **1**, 444–451 (2018).
41. Solomon, J. B. et al. Probing the all-ferrous states of methanogen nitrogenase iron proteins. *JACS Au* **1**, 119–123 (2020).
42. Solomon, J. B. et al. Heterologous expression of a fully active *Azotobacter vinelandii* nitrogenase Fe protein in *Escherichia coli*. *mBio* **14**, e0257223 (2023).
43. Quechol, R. et al. Heterologous synthesis of the complex homometallic cores of nitrogenase P- and M-clusters in *Escherichia coli*. *Proc. Natl Acad. Sci. USA* **120**, e2314788120 (2023).
44. Dixon, R. A. & Postgate, J. R. Genetic transfer of nitrogen fixation from *Klebsiella pneumoniae* to *Escherichia coli*. *Nature* **237**, 102–103 (1972).
45. Wang, L. et al. A minimal nitrogen fixation gene cluster from *Paenibacillus* sp. WLY78 enables expression of active nitrogenase in *Escherichia coli*. *PLoS Genet.* **9**, e1003865 (2013).
46. Yang, J., Xie, X., Wang, X., Dixon, R. & Wang, Y.-P. Reconstruction and minimal gene requirements for the alternative iron-only nitrogenase in *Escherichia coli*. *Proc. Natl Acad. Sci. USA* **111**, E3718–E3725 (2014).
47. Deere, T. M., Prakash, D., Lessner, F. H., Duin, E. C. & Lessner, D. J. *Methanosarcina acetivorans* contains a functional ISC system for iron–sulfur cluster biogenesis. *BMC Microbiol.* **20**, 323 (2020).
48. Angove, H. C., Yoo, S. J., Münck, E. & Burgess, B. K. An all-ferrous state of the Fe protein of nitrogenase. Interaction with nucleotides and electron transfer to the MoFe protein. *J. Biol. Chem.* **273**, 26330–26337 (1998).
49. Pierik, A. J., Wassink, H., Haaker, H. & Hagen, W. R. Redox properties and EPR spectroscopy of the P clusters of *Azotobacter vinelandii* MoFe protein. *Eur. J. Biochem.* **212**, 51–61 (1993).
50. Gao, D., Huang, X. & Tao, Y. A critical review of NanoSIMS in analysis of microbial metabolic activities at single-cell level. *Crit. Rev. Biotechnol.* **36**, 884–890 (2016).
51. Popa, A. et al. Carbon and nitrogen fixation and metabolite exchange in and between individual cells of *Anabaena oscillarioides*. *ISME J.* **1**, 354–360 (2007).
52. Noar, J. D. & Bruno-Bárcena, J. M. *Azotobacter vinelandii*: the source of 100 years of discoveries and many more to come. *Microbiology (Reading)* **164**, 421–436 (2018).
53. Zheng, L., Kostrewa, D., Bernèche, S., Winkler, F. K. & Li, X. D. The mechanism of ammonia transport based on the crystal structure of AmtB of *Escherichia coli*. *Proc. Natl Acad. Sci. USA* **101**, 17090–17095 (2004).
54. Kleiner, D. Bacterial ammonium transport. *FEMS Microbiol. Rev.* **32**, 87–100 (1985).
55. Nielander, A. C. et al. A versatile method for ammonia detection in a range of relevant electrolytes via direct nuclear magnetic resonance techniques. *ACS Catal.* **9**, 5797–5802 (2019).
56. Kuchenreuther, J. M. et al. High-yield expression of heterologous [FeFe] hydrogenases in *Escherichia coli*. *PLoS One* **5**, e15491 (2010).
57. Akhtar, M. K. & Jones, P. R. Deletion of iscR stimulates recombinant clostridial Fe–Fe hydrogenase activity and H_2-accumulation in *Escherichia coli* BL21(DE3). *Appl. Microbiol. Biotechnol.* **78**, 853–862 (2008).
58. Burgess, B. K., Jacobs, D. B. & Stiefel, E. I. Large-scale purification of high activity *Azotobacter vinelandii* nitrogenase. *Biochim. Biophys. Acta* **614**, 196–209 (1980).
59. Newcomb, M. P. et al. A V-nitrogenase variant containing a citrate-substituted cofactor. *ChemBioChem* **21**, 1742–1748 (2020).
60. Liedtke, J. et al. Characterization of a Mo-nitrogenase variant containing a citrate-substituted cofactor. *ChemBioChem* **22**, 151–155 (2021).
61. Fay, A. W., Lee, C. C., Wiig, J. A., Hu, Y. & Ribbe, M. W. Protocols for cofactor isolation of nitrogenase. *Methods Mol. Biol.* **766**, 239–248 (2011).

Acknowledgements

This work was supported by NIH-NIGMS grant GM67626 (to M.W.R. and Y.H.), which funded research related to nitrogenase assembly, NIH-NIGMS grant GM141046 (to Y.H. and M.W.R.), which funded research related to nitrogenase mechanism, and Department of Energy grant DOE (BES) DE-SC0016510 (to Y.H. and M.W.R.), which funded work related to the mechanistic investigation of ammonia formation through the engineering of nitrogenase proteins.

Author contributions

J.B.S. and C.C.L. designed experiments, performed experiments and analysed data. Y.A.L. and C.D. performed experiments. M.W.R. and Y.H. designed experiments, analysed data and wrote the manuscript.

Competing interests

The authors declare no competing interests.

Additional information

Supplementary information The online version contains supplementary material available at https://doi.org/10.1038/s41929-024-01229-x.

Correspondence and requests for materials should be addressed to Markus W. Ribbe or Yilin Hu.

Peer review information *Nature Catalysis* thanks Xavier Mayali and the other, anonymous, reviewer(s) for their contribution to the peer review of this work.

nature portfolio

Corresponding author(s): Markus W. Ribbe, Yilin Hu

Last updated by author(s): August 6, 2024

Reporting Summary

Nature Portfolio wishes to improve the reproducibility of the work that we publish. This form provides structure for consistency and transparency in reporting. For further information on Nature Portfolio policies, see our Editorial Policies and the Editorial Policy Checklist.

Statistics

For all statistical analyses, confirm that the following items are present in the figure legend, table legend, main text, or Methods section.

n/a	Confirmed
☐	☒ The exact sample size (*n*) for each experimental group/condition, given as a discrete number and unit of measurement
☒	☐ A statement on whether measurements were taken from distinct samples or whether the same sample was measured repeatedly
☒	☐ The statistical test(s) used AND whether they are one- or two-sided *Only common tests should be described solely by name; describe more complex techniques in the Methods section.*
☒	☐ A description of all covariates tested
☒	☐ A description of any assumptions or corrections, such as tests of normality and adjustment for multiple comparisons
☐	☒ A full description of the statistical parameters including central tendency (e.g. means) or other basic estimates (e.g. regression coefficient) AND variation (e.g. standard deviation) or associated estimates of uncertainty (e.g. confidence intervals)
☒	☐ For null hypothesis testing, the test statistic (e.g. *F*, *t*, *r*) with confidence intervals, effect sizes, degrees of freedom and *P* value noted *Give P values as exact values whenever suitable.*
☒	☐ For Bayesian analysis, information on the choice of priors and Markov chain Monte Carlo settings
☒	☐ For hierarchical and complex designs, identification of the appropriate level for tests and full reporting of outcomes
☒	☐ Estimates of effect sizes (e.g. Cohen's *d*, Pearson's *r*), indicating how they were calculated

Our web collection on statistics for biologists contains articles on many of the points above.

Software and code

Policy information about availability of computer code

Data collection	No software was used for data collection
Data analysis	EasySpin 5.2.27 toolbox; L'image

For manuscripts utilizing custom algorithms or software that are central to the research but not yet described in published literature, software must be made available to editors and reviewers. We strongly encourage code deposition in a community repository (e.g. GitHub). See the Nature Portfolio guidelines for submitting code & software for further information.

Data

Policy information about availability of data

All manuscripts must include a data availability statement. This statement should provide the following information, where applicable:

- Accession codes, unique identifiers, or web links for publicly available datasets
- A description of any restrictions on data availability
- For clinical datasets or third party data, please ensure that the statement adheres to our policy

All data is available from the authors upon reasonable request.

Research involving human participants, their data, or biological material

Policy information about studies with human participants or human data. See also policy information about sex, gender (identity/presentation), and sexual orientation and race, ethnicity and racism.

Reporting on sex and gender	N/A
Reporting on race, ethnicity, or other socially relevant groupings	N/A
Population characteristics	N/A
Recruitment	N/A
Ethics oversight	N/A

Note that full information on the approval of the study protocol must also be provided in the manuscript.

Field-specific reporting

Please select the one below that is the best fit for your research. If you are not sure, read the appropriate sections before making your selection.

☒ Life sciences ☐ Behavioural & social sciences ☐ Ecological, evolutionary & environmental sciences

For a reference copy of the document with all sections, see nature.com/documents/nr-reporting-summary-flat.pdf

Life sciences study design

All studies must disclose on these points even when the disclosure is negative.

Sample size	N/A; biological replicates are described but not expressed as n
Data exclusions	No data presented herein were excluded from the analyses but instead stated in the figure and table captions
Replication	(1) Figure 2c,d; Supplementary Table 3: Metal and activity assays were each performed on three independent samples. Shown in the figure are mean+/-s.d. (2) Figure 3d,e; Supplementary Table 4: Metal and activity assays were each performed on four to six independent samples. Shown in the figure are mean+/-s.d. (3) Figure 4d:; Supplementary Table 5: Activity analyses were performed on three to six independent samples. Shown in the figure are mean +/-s.d. (4) Figure 5a; Supplementary Table 5: Metal analyses were each performed on three independent samples. Shown in the figure are mean+/-s.d. (5) Figure 6a,b: Cell growth experiments were performed six times. Shown in the figure are OD (600 nm) readings as mean+/-s.e.m. (6) Figure 7b-e; Supplementary Figure 4: NanoSIMS analyses were each conducted on one to seven independent samples. (7) Figure 8c,d: NanoSIMS analyses were each conducted on one sample. (8) Supplementary Figure 5: Nano SIMS analyses were each conducted on one sample.
Randomization	N/A
Blinding	N/A

Reporting for specific materials, systems and methods

We require information from authors about some types of materials, experimental systems and methods used in many studies. Here, indicate whether each material, system or method listed is relevant to your study. If you are not sure if a list item applies to your research, read the appropriate section before selecting a response.

Materials & experimental systems

n/a	Involved in the study
☒	☐ Antibodies
☒	☐ Eukaryotic cell lines
☒	☐ Palaeontology and archaeology
☒	☐ Animals and other organisms
☒	☐ Clinical data
☒	☐ Dual use research of concern
☒	☐ Plants

Methods

n/a	Involved in the study
☒	☐ ChIP-seq
☒	☐ Flow cytometry
☒	☐ MRI-based neuroimaging

Plants

Seed stocks	N/A
Novel plant genotypes	N/A
Authentication	N/A